ELSEVIER

Catalysis Today 51 (1999) 233–254

CATALYSIS TODAY

Titania–silica as catalysts: molecular structural characteristics and physico-chemical properties

Xingtao Gao, Israel E. Wachs*

Department of Chemistry and Chemical Engineering, Zettlemoyer Center for Surface Studies, Lehigh University, 7 Asa Drive, Bethlehem, PA 18015, USA

Abstract

Recent results on characterization and applications of titania–silica materials as photocatalysts, acid catalysts and oxidation catalysts are reviewed. The similarities and differences in structural characteristics and physico-chemical properties between titania–silica mixed and supported oxides are emphasized. The generation of new catalytic active sites either on the silica surface or in the silica matrix is discussed with respect to the formation of Ti–O–Si bonds and the local structure. The insights obtained from these studies allow a fundamental understanding of the relationships between the structural characteristics and the physico-chemical/reactivity properties of titania–silica catalysts.

Keywords: TiO_2–SiO_2 mixed oxides; TiO_2/SiO_2 supported oxides; Catalyst; Glass; Sol–gel; Multilayers/thin films; Surface structure; Coordination geometry; Electronic property; Photocatalysis; Acidity; Epoxidation and oxidation reactions; Isomerization and dehydration reactions; EXAFS/XANES; UV–Vis DRS; Raman; IR; XPS spectroscopy

1. Introduction

Titania–silica represents a novel class of materials that have attracted much attention in recent years. Titania–silica materials have been extensively used as catalysts and supports for a wide variety of reactions [1–48], as summarized in Table 1. In addition, titania–silica can be utilized as protective coating on stainless steel to resist oxidation and chemical attack [49,50], antireflection coatings for optical glasses [51], and as very interesting glass materials with ultralow thermal expansion coefficients [52–57] and high refraction indices [58]. Such advanced titania–silica materials not only take advantage of both TiO_2 (an *n*-type semiconductor and an active catalytic support) and SiO_2 (high thermal stability and excellent mechanical strength), but also extends their applications through the generation of new catalytic active sites due to the interaction of TiO_2 with SiO_2.

The applications of titania–silica materials as catalysts and supports fall into three categories based on their unique physico-chemical properties: (i) photocatalysis that is associated with the support effect and the quantum-size effect; (ii) acid catalysis that is related to the generation of new acid sites; and (iii) excellent catalytic support materials that possess enhanced thermal and mechanical stability due to SiO_2 while preserving the catalytic performance of TiO_2. The understanding of the structural characteristics of titania–silica and the relationships with the physico-chemical/reactivity properties is also of great importance in a wide range of applied sciences. This

*Corresponding author. Tel.: +1-610-758-4274; fax: +1-610-758-6555; e-mail: iew0@lehigh.edu

0920-5861/99/$ – see front matter
PII: S0920-5861(99)00048-6

Table 1
Summary of various reactions for titania–silica as catalysts and supports

Catalysts	Preparation method	Reaction temperature (K)	Reactions	Reference
TiO_2–SiO_2	Sol–gel	RT	Photodecomposition of chlorinated phenols	[1,2]
TiO_2–SiO_2	Sol–gel/CVD	RT	Photoreduction of CO_2	[3,4]
TiO_2–SiO_2	Sol–gel	RT	Photodecomposition of rhodamine-6G and phenol	[5,6]
TiO_2–SiO_2	Sol–gel	380	Complete photocatalytic oxidation of C_2H_4	[7]
TiO_2/SiO_2	Impregnation	RT	Photoxidation of propane	[8]
TiO_2/SiO_2	Precipitation	673	Catalytic decomposition of 1,2-dichloroethane	[9]
TiO_2–SiO_2	–	823	Catalytic decomposition of Freon 12	[10]
TiO_2/SiO_2	Precipitation	523–673	Catalytic decomposition of chloroform	[11]
TiO_2–SiO_2	Sol–gel/coprecipitation	423–523	Isomerization of 1-butene	[12–18]
TiO_2–SiO_2	Sol–gel	523	Isomerization of methyloxane to propanal	[18]
TiO_2–SiO_2	Sol–gel/coprecipitation	–	Methanol dehydration	[19]
TiO_2–SiO_2	Coprecipitation	493	Ethene hydration	[15]
TiO_2–SiO_2	Coprecipitation	723	Phenol amination	[15]
TiO_2–SiO_2	Coprecipitation	673	Cumene dealkylation	[20]
TiO_2–SiO_2	Sol–gel	–	Decane hydrocracking	[21]
TiO_2–SiO_2	Sol–gel/impregnation	–	Propanol dehydration	[12,20,36,37]
TiO_2–SiO_2	Coprecipitation	303	Solvolysis of *cis*-2,3-epoxybutane	[22]
TiO_2–SiO_2	Sol–gel	493	Ammoxidation of cyclohexanone	[23]
TiO_2–SiO_2	Sol–gel	333	Epoxidation of α-isophorone by TBHP	[24,25]
TiO_2–SiO_2	Sol–gel/coprecipitation	323–363	Epoxidation of olefins by TBHP/NBHP/H_2O_2	[21,22,26–31]
TiO_2/SiO_2	Impregnation	363–383	Epoxidation of olefins by TBHP/EBHP	[31–33]
TiO_2–SiO_2	Sol–gel	353	Selective oxidation of cyclohexane by TBHP	[34]
TiO_2–SiO_2	Sol–gel	353	Hydroxylation of phenol by H_2O_2	[35]
TiO_2–SiO_2	Sol–gel	353	Oxidation of benzene and toluene by H_2O_2	[35]
TiO_2/SiO_2	Impregnation	503	Methanol oxidation	[36,38]
Rh/TiO_2–SiO_2	Sol–gel	303	Benzene hydrogenation	[39]
Ni/TiO_2–SiO_2	Coprecipitation	548	CO hydrogenation	[14]
CrO_3/TiO_2–SiO_2	Coprecipitation/impregnation	373–383	Ethylene polymerization	[40,41]
V_2O_5/TiO_2–SiO_2	Sol–gel/impregnation	370–570	SCR of NO with NH_3	[42–44]
V_2O_5/TiO_2–SiO_2	Coprecipitation	353	Synthesis of isobutyaldehyde from ethanol+methanol	[45]
V_2O_5/TiO_2/SiO_2	Precipitation	423–823	NO reduction with CO	[46]
V_2O_5/TiO_2/SiO_2	Precipitation	600–700	Selective oxidation of toluene	[47]
V_2O_5/TiO_2/SiO_2	Precipitation	533–673	Selective oxidation of *o*-xylene	[48]

review focuses on the investigation and development of amorphous titania–silica mixed and supported oxides as catalysts, excluding Ti-silicalites, over the past 10 years with special emphasis on the structural characterization and establishment of the relationships between the structural characteristics and the physico-chemical/reactivity properties.

Comparison of the various results in the literature between different researchers is sometimes difficult because of different preparation methods, sample treatments, and characterization techniques used to determine the structural and surface properties. In spite of this situation, we will try to provide a consistent picture to clarify the structure–property relationships for titania–silica materials based on the combined results of different characterization techniques and researchers.

2. Interaction of TiO_2 with SiO_2

There are two types of interaction between TiO_2 and SiO_2: physically mixed (with interaction forces being nothing more than weak Van der Waals forces) and chemically bonded (i.e., the formation of Ti–O–Si linkages). When strong interaction results in chemical bonding, the physico-chemical/reactivity properties of titania–silica are very different from the simple combination of the individual phases (mechanical mixtures). The degree of interaction, or in other words homogeneity or dispersion, largely depends on preparation methods and synthesis conditions (see below). Many different preparation methods have been employed to synthesize titania–silica. The most widely used methods to prepare TiO_2–SiO_2 mixed oxides and glasses are sol–gel hydrolysis [1,3,5–7,10,12,26–30,35,39,42,44,49,50,59–64], coprecipitation [15,16,19,20,22,45,65], and flame hydrolysis [66–68]. The supported oxides of TiO_2 deposited on the SiO_2 substrate, denoted as TiO_2/SiO_2 supported oxides, have been much less investigated and are prepared by impregnation [8,36–38,69–76], chemical vapor deposition [77–79] and precipitation [11,71,72,76,80]. The interaction of TiO_2 with SiO_2 at the interface of TiO_2/SiO_2 multilayers/thin films as one type of supported oxides will also be addressed in order to have a clearer overview about the intrinsic nature of interaction between TiO_2 and SiO_2. The general term *titania–silica* is used to include both mixed and supported oxides.

2.1. TiO_2–SiO_2 mixed oxides

2.1.1. Preparation of TiO_2–SiO_2 mixed oxides

TiO_2–SiO_2 mixed oxides are generally prepared by sol–gel and coprecipitation methods. Two types of Ti species are present in TiO_2–SiO_2 mixed oxides: segregated TiO_2 microdomains and isolated Ti species, with the relative ratio depending on the chemical composition, the preparation methods and synthesis conditions (the hydrolysis route, Ti content, drying method and calcination temperature) [13,31,81]. The degree of homogeneity at the atomic level is commonly associated with the relative amount of Ti–O–Si linkages in TiO_2–SiO_2 mixed oxides [12,13,19,26,31,64,82,83], and Ti–O–Si bonds are more effectively formed as the homogeneity increases.

Among the various preparation methods, sol–gel hydrolysis is most widely used due to its possible capability in controlling the textural and surface properties of the mixed oxides. In sol–gel processes, domain formation due to the differences in the hydrolysis and the condensation rates of Ti- and Si- alkoxides was identified to be a major problem in the preparation of atomically mixed TiO_2–SiO_2 oxides [82]. However, the two-stage hydrolysis procedure recently developed, which is performed in acidic conditions, seems to have overcome this problem and results in the best Ti–O–Si connectivities and the highest homogeneity [13,62,82].

Although the homogeneity of TiO_2–SiO_2 mixed oxides varies with the preparation methods and synthesis conditions, the atomically mixed TiO_2–SiO_2 oxides can only be obtained at low TiO_2 content, with the maximum TiO_2 concentration less than 15 wt% [65,68], or Si/Ti atomic ratio higher than 7.5. At higher Ti contents, TiO_2 crystallites tend to form as a separate phase, demonstrating that silica could not favorably accommodate all the Ti atoms in the network above a certain limit.

2.1.2. Experimental evidence for Ti–O–Si bonding

The presence of Ti–O–Si linkages in TiO_2–SiO_2 mixed oxides has been detected directly or indirectly by many techniques, such as XPS [65,67], EXAFS/XANES spectroscopy [27–29,68,81,84,85], IR and

Raman spectroscopy [62,64,82,86–88], ^{29}Si and ^{17}O NMR spectroscopy [26,35,61–63,89].

The simplest way to examine the formation of Ti–O–Si bonds is to use IR spectroscopy. The IR band observed at 910–960 cm^{-1} is widely accepted as the characteristic vibration due to the formation of Ti–O–Si bonds [30,35,62,64,81,82,86–88], with the exact band position depending on the chemical composition of the sample as well as calibration and resolution of the instrument. The intensity of this IR band has been used to evaluate the absolute amount of Ti–O–Si linkages [62,64,82,86–88], which has been shown to increase with increasing Ti content up to 20 wt% TiO_2 [64]. The dispersion of Ti in the SiO_2 matrix has been associated with the ratio of IR vibration due to Ti–O–Si bond at 930–960 cm^{-1} to that due to Si–O–Si at ca. 1210 cm^{-1} [30,64]. However, IR spectroscopy is not sensitive to the formation of TiO_2 crystallites.

Raman studies of TiO_2–SiO_2 mixed oxides provide additional evidence for the assignment of the vibrational modes of the Ti–O–Si bond. The Raman spectra of TiO_2–SiO_2 mixed oxides show two bands at 935–960 and 1100–1110 cm^{-1} [35,38,62,84,86,88], which are associated with vibrational modes involving Ti–O–Si bonding (the assignment of the vibrational modes will be discussed in detail below in Section 2.3). Raman spectroscopy, with especially a multichannel analyzer, is extremely sensitive to the presence of TiO_2 crystallites. The formation of TiO_2 crystallites (anatase) can be recognized by a sharp Raman band at ~144 cm^{-1} with a minimum detectable amount of 0.05 wt% TiO_2 [85]. Interestingly, at Ti content above 10 mol%, Best et. al [84] observed a Raman band at ~665 cm^{-1}, which was assigned to Ti(IV) in fivefold or sixfold coordination. An IR band has been also observed at ~665 cm^{-1}, and the authors only assigned it to the Ti–O–Si vibration [87]. However, this particular vibrational band was never observed by other authors [64,82,86,88].

XPS analysis also reveals the strong interaction between TiO_2 and SiO_2 in the mixed oxides [35,65]. The Ti $2p_{3/2}$ binding energy (BE) at low titania content (<10 wt%) is ~460 eV, which is higher than the value for pure TiO_2 (~458.7 eV) [65]. This upward shift has been explained by the increase in the interatomic potentials due to the decrease of the coordination number of Ti and the shortening of the Ti–O bond, which suggests the insertion of Ti^{4+} cations into tetrahedral sites of the silica network [65,67,90]. However, since the Ti atoms are less electronegative and more polarizable than the Si atoms, this shift could also be accounted for by the increase of the effective positive charge on the Ti atoms due to the Ti–O–Si bonds. This latter explanation is supported by the observation that BE values of both O1s and Si 2p shift downward, indicative of a decrease in the effective positive charge on Si and an increase in the negative charge on O due to the formation of Ti–O–Si bonds [65]. As will be shown later in Section 2.2, TiO_2/SiO_2 supported oxides and multilayers/thin films also show similar shifts, suggesting that the changes in BE values of Ti, Si and O are associated with the formation of Ti–O–Si linkages that are common in these systems.

^{29}Si NMR spectroscopy has been applied to study the changes in the SiO_2 structure when Ti atoms are incorporated into the silica network [26,35,61–63]. Broadband decoupled spectra yield the percentage of Q^2, Q^3 and Q^4 sites, where Q^n denotes a ^{29}Si nucleus with a $Si(OSi)_n(OX)_{4-n}$ local environment (X=H or Ti) [62,63]. The contributions from Ti–O–Si bridges for Q^2 and Q^3 sites were found to be dominant in the sol–gel prepared mixed oxides [26,63]. However, this technique cannot provide quantitative information about the Ti–O–Si linkages because the ^{29}Si resonances from Si–O–H and Si–O–Ti bonds are not distinguishable. In addition, this technique is not sensitive to the presence of crystalline TiO_2 [61–63].

Direct information about Ti–O–Si linkages in TiO_2–SiO_2 gels can be obtained with ^{17}O NMR spectroscopy [61,89]. A chemical shift at δ 280–260 is observed for Ti–O–Si that is intermediate between the chemical shifts of Si–O–Si and Ti–O–Ti. This resonance is uniquely assigned to the oxygen atoms in Ti–O–Si linkages, which offers the possibility to determine the numbers of different oxide linkage quantitatively [89].

All the above characterization results confirm the formation of Ti–O–Si linkages in TiO_2–SiO_2 mixed oxides.

2.1.3. *Characterization of the local structure of the Ti atoms in the SiO_2 matrix*

To determine the local structure of Ti(IV) in amorphous TiO_2–SiO_2 mixed oxides (where TiO_2 crystallites are not present to complicate the analysis), the

physical techniques used should possess the ability to probe short-range order. Neutron diffraction and X-ray diffraction [91,94], extended X-ray absorption fine structure (EXAFS) and X-ray absorption near edge spectroscopy (XANES) [27–29,68,81,84,85] and UV–Vis [60,79,81,93,94] spectroscopy have been employed to establish the coordination geometry of the Ti atoms in the SiO_2 matrix.

Ti K-edge EXAFS/XANES has been shown to be very powerful in studying the local structure of Ti in amorphous TiO_2–SiO_2 mixed oxides. From the EXAFS experiment, the Ti–O, Ti–Si and Ti–Ti bond lengths and the coordination number around Ti can be obtained. The XANES pre-edge features provide additional formation about the coordination geometry of Ti. Ti atoms in tetrahedral sites without inversion symmetry exhibit strong pre-edge absorption features, and Ti atoms in octahedral sites give rise to a very small or no pre-edge absorption features. Early EXAFS/XANES studies by Greegor et al. [68,95] suggested that the Ti atoms in TiO_2–SiO_2 glasses possess predominantly tetrahedral coordination in the range 0.05–9 wt% TiO_2 with a small amount of Ti in octahedral coordination (less than 5% of the total Ti atoms). Increasing concentration of TiO_2 up to 15 wt% increases the sixfold/fourfold ratio, and crystalline TiO_2 aggregates were found as a second phase at ca. 15 wt% TiO_2. They obtained an average bond length of 1.81 Å for the tetrahedrally coordinated Ti–O and 1.99 Å for the octahedrally coordinated Ti–O [68]. Similar conclusions have been described by Liu et al. [81] with an average Ti–O bond distance of 1.82 Å at a low Ti content (Ti/Si=1/8.2). Moreover, a strong pre-edge peak intensity (58–75%) for these TiO_2–SiO_2 mixed oxides at low Ti contents further confirms that Ti atoms are located predominantly in tetrahedral sites [68,81].

It should be pointed out that the pre-edge peak intensity alone is not sufficient to make the unambiguous assignment of the Ti coordination since similar peak intensity can arise from Ti in fourfold and fivefold coordinations as well as sixfold coordination with Ti in highly distorted oxygen octahedra [96]. As will be discussed in detail later (Section 2.3.2), both the pre-edge position and the normalized height should be used to correctly determine the Ti coordination. However, the combined results from both EXAFS and XANES experiments, which reveal the average short Ti–O distance of ∼1.80 Å and a strong pre-edge peak, strongly suggest that the Ti atoms mostly reside in the tetrahedral sites at low Ti content (<15 wt% TiO_2).

Rosenthal et al. [97] have performed a molecular dynamics computer simulation study of TiO_2–SiO_2 glasses. They obtained an average Ti–O bond length of 1.77 Å for the tetrahedral coordination and 1.96 Å for the octahedral coordination, which is in agreement with the above EXAFS results. Interestingly, the results from the computer simulation also suggests the presence of fivefold coordination of Ti with an average Ti–O bond length of 1.87 Å. However, a small amount of fivefold coordination of Ti is very difficult to identify by EXAFS/XANES or other characterization techniques because a mixture of fourfold and sixfold coordination may give rise to similar features.

Walters et al. [91] applied neutron diffraction experiment to study the local environment of Ti in the silica matrix as well as the influence of Ti on the silica network. They found that at low Ti contents, Ti is in fourfold coordination with an average Ti–O bond length of ∼1.8 Å, consistent with the EXAFS results. Moreover, the silica network is significantly affected with the Si–O bond-length distributions being narrowed and a high level of network –OH. The authors argued that the effect of the larger Ti atom as compared to the Si atom will produce some distortion of the SiO_4 tetrahedral network, therefore increasing the amount of network strain which may give rise to a high –OH content when the strain is relieved. The authors suggest that the most important effect of Ti on the macroscopic structure of these materials is the effect of the network-terminating/modifying of O–H bond.

Rigden et al. [92] have tried to use X-ray diffraction to get some structural information about TiO_2–SiO_2 mixed oxides. However, the bond length obtained for the fourfold coordinated Ti atom is averaged over 1.4–1.9 Å. Due to its low sensitivity, X-ray diffraction cannot distinguish between first-neighbor Si–O and Ti–O distances and cannot measure quantitatively the small differences in structure between the pure silica and titania–silica [92].

UV–Vis spectroscopy is a very useful tool to investigate the band structure of TiO_2–SiO_2 mixed oxides at the molecular energy level. Blue shifts of bandgap absorption edges are always observed at low Ti contents. The contributions to the increase of the bandgap

energy may result from (i) the quantum size effect and (ii) the matrix/support effect. The well known quantum size effect is expected to be detectable for semiconductor titania at the nano-sized level [98]. In order to discriminate between the two effects, it is important to first use other techniques such as Raman spectroscopy to identify the types of titanium oxide species, otherwise, this technique may not provide very valuable information about the molecular structure of Ti species due to the complexity introduced by simultaneously having multiple Ti species.

The UV–Vis DRS spectra may provide some information on the first and the second coordination spheres of Ti. Following the literature [99], the charge transfer transitions (LMCT) between the ligand (X=H–O^-, Si–O^-, Ti–O^-, etc.) and the empty d-orbital of Ti^{4+} can be estimated from the optical electronegativities χ of ligand X and Ti^{4+} by the following equation:

$$\bar{\nu}(\mathrm{cm}^{-1}) = 30\,000[\chi_{\mathrm{opt}}(X) - \chi_{\mathrm{opt}}(\mathrm{Ti})]. \quad (1)$$

On one hand, the increase of the coordination of Ti from tetrahedral to octahedral increases the χ_{opt}(Ti) value from 1.85 to 2.05 [99]. The LMCT band for Ti in octahedral sites is supposedly at a lower wavenumber compared to that of Ti in tetrahedral sites. For example, the LMCT transitions of the well-documented TS-1 are observed at 50 000–48 000 cm^{-1} that are assigned to Ti in isolated tetrahedral sites [90], while the LMCT transitions of Ti in octahedral sites of anatase are often observed at 30 000 cm^{-1}. Therefore, in some cases, the above equation could be used to justify the coordination of Ti. On the other hand, the coordination change is usually accompanied by a change in the second coordination sphere (ligands). For example, the coordination change due to hydration of tetrahedral Ti sites is only partially responsible for the downward shift of the LMCT band [81,93,100]. Unfortunately, the electronegativity values (χ_{opt}(X)) of oxygenated ligands are quite arbitrary in the literature: Si–O^- (χ_{opt}=3.17) and H–O^- ligands (χ_{opt}=2.9) [101], X–O^- ligands (χ_{opt}=3.45, X=H–O^- and O^{2-}) [93,100], H_2O ligand (χ_{opt}=3.5) [101]. The ligand change in the coordination sphere of tetrahedral Ti from Si–O^- to H–O^- due to hydration is estimated to redshift the LMCT band by ~8000 cm^{-1}, according to Eq. (1)[60,99]. However, the redshift of the LMCT transitions of Ti observed for Ti-silicalite and TiO_2–SiO_2 mixed oxides [60,93,100] upon hydration is usually in the range 1000–6000 cm^{-1}, and is a combined effect of both the increased coordination number and the change in ligand. Thus, it is difficult for a single value of the optical electronegativity to properly represent the Ti atoms in different coordination and ligand environments.

Furthermore, it has been shown that the ligand environments of Ti can play a major role in determining the LMCT transitions [102]. Three Ti-reference compounds with different coordination and ligands are compared. Ba_2TiO_4 possesses isolated TiO_4 tetrahedra linked by Ba atoms, JDF-L1 ($Na_4Ti_2Si_8O_{22}.4H_2O$) and Ti-umbite ($K_2TiSi_3O_9.H_2O$) contain isolated TiO_5 square pyramids and isolated TiO_6 octahedra with Ti–O–Si linkages, respectively. The LMCT transitions of Ti cations decrease in the order: JDF-L1>Ti-umbite>Ba_2TiO_4, which is in contrast to the expectation that Ba_2TiO_4 with fourfold coordination would display the highest LMCT transitions. The actual lowest LMCT transitions of the Ti atoms in Ba_2TiO_4 can be accounted for by Ba atoms as the second coordination sphere that are much less electronegative than Si atoms as the second coordination sphere of Ti atoms in JDF-L1 and Ti-umbite. Therefore, it is practically not possible to apply Eq. (1) to quantitatively calculate the shift of the LMCT transitions upon the change in coordination and ligand environments.

A comparative study on the molecular structures of 1.5 wt% TiO_2–SiO_2 mixed oxide and TS-1 by UV–Vis spectroscopy has been performed by On et al. [60] (in both samples, Ti is in tetrahedral sites with the same low Ti content). The LMCT transition of tetrahedral Ti in the dehydrated TS-1 was deconvoluated into three components centered at 50 200, 44 060 and 40 290 cm^{-1} [60,94]. Whereas the LMCT band for the dehydrated TiO_2–SiO_2 mixed oxide was centered at 40 000 cm^{-1}, which is ~10 000 cm^{-1} lower than that of TS-1. Since the Ti atoms in both samples reside in tetrahedral sites, the authors argue that a large average Ti–O–Si bond angle of 163° in TS-1 as compared to 159° in the mixed oxides [68,94] may result in a higher π donation, contributing to the higher LMCT transition energy. Thus, they suggest that Ti in TiO_2–SiO_2 mixed oxides is located more in closed sites Ti$(OSi)_4$ with a smaller bond angle, while Ti in TS-1 is located more in open sites Ti$(OH)(OSi)_3$.

However, Klein et al. [93] observed an absorption at 45 000 cm^{-1} for dehydrated TiO_2–SiO_2 mixed oxides at a low Ti concentration, and this band shifts slightly downward to ca. 41 000 cm^{-1} with increasing Ti concentration up to 9 mol%. This LMCT band was simply assigned to the isolated tetrahedral Ti species. The LMCT transition assigned to tetrahedral Ti species in TiO_2–SiO_2 mixed oxides [26,60,93] is often observed at a lower wavenumber than in TS-1. It is very unlikely that this difference is due to the so-called open and closed sites, since ammonia adsorption results show that a large fraction of tetrahedral Ti atoms in TiO_2–SiO_2 mixed oxides at low Ti contents are located around the surface [12] which is the right location for the open sites. However, the presence of a small fraction of octahedral Ti species in the mixed oxides even at very low Ti contents [12,68], together with the possible presence of some Ti–O–Ti linkages (no experimental results have shown that all Ti atoms in TiO_2–SiO_2 mixed oxides are isolated), might account for this difference.

All results point toward the substitution of Ti as a tetrahedral species for Si in the silica network at low Ti content, and that the fraction of tetrahedral Ti atoms decreases as the Ti content increases [26]. Furthermore, the degree of disorder of the Ti–O bond lengths and Ti–O–Si angles seems substantially higher compared to the framework Ti atoms in crystalline TS-1 [85].

The effect of water vapor on the coordination geometry of the Ti atoms in atomically mixed TiO_2–SiO_2 oxides has been examined by XANES and UV–Vis spectroscopies [60,81]. XANES experiment demonstrated that the coordination environment of Ti is dramatically affected by the coordination of water vapor, since the pre-edge feature doubled after dehydration [81]. UV–Vis spectroscopy also shows the coordination change upon hydration since the LMCT band for TiO_2–SiO_2 mixed oxides shifts downward for ~1000 cm^{-1} [60]. In these cases the coordination of Ti is supposed to change from fourfold to five or sixfold upon water addition.

2.2. TiO_2/SiO_2 supported oxides

2.2.1. Preparation of TiO_2/SiO_2 supported oxides

In order to improve the mechanical strength, thermal stability and surface area of TiO_2, TiO_2/SiO_2 supported oxides have been considered as an advanced support material to replace pure TiO_2 [36,37,46–48,71,72,75,76]. Unlike the substitution of Ti for Si in the silica network in the mixed oxides, the interaction of TiO_2 with the silica support is limited to the surface, which is one of surface modifications of silica by chemical reactions [36,37,77,78,102].

It is well known that the silica surface is quite inert, and it is very difficult to synthesize highly dispersed metal oxides on the silica surface. Of all the chemical modification reactions on silica, the surface hydroxyls generally act as the adsorptive/reactive sites because of their hydrophilic character. Thus, the preparation of highly dispersed metal oxides on silica by either impregnation or the chemical vapor deposition method often involves a highly reactive precursor, such as $TiCl_4$ or Ti-alkoxides, to react with the surface hydroxyls on silica [36,37,74,75,77–79,102]. The titration of the surface hydroxyls with Ti-precursors is either monofunctional (one Ti-alkoxide molecule titrating one OH group) or bifunctional (one Ti-alkoxide molecule titrating two OH group) depending on the pretreatment temperature, the reaction temperature, and the size and reactivity of the precursor [77,78,102]. Thus, the Ti atoms bind to the silica surface via oxygen as a bridge. Two types of Ti species, highly dispersed surface TiO_x species and TiO_2 crystallites, are possibly present on the silica surface, depending on the preparation conditions and chemical compositions [37,75,77,102].

The dispersion capacity is closely related to the concentration of hydroxyls on the silica surface and the preparation conditions (e.g., the pretreatment temperature, the reaction/impregnation time, the reactivity and molecular size of the precursor) [37,75,77,78,102]. A maximum dispersion of TiO_2 was reached at ~3.0 Ti/nm^2 on a non-porous SiO_2 (Stöber silica spheres) due to its highest concentration of surface hydroxyls and highest accessibility to the reagent [37]. However, a recent study [102] shows that a maximum capacity of highly dispersed TiO_x species on silica can be reached at ~4.0 Ti atom/nm^2 by carefully controlling the above preparation variables. This maximum capacity seems correlated with the surface concentration of OH groups on silica, suggesting a maximum coverage of surface TiO_x species on the silica surface.

2.2.2. Experimental evidence for Ti–O–Si bonding

In contrast to the large number of research papers on TiO_2–SiO_2 mixed oxides, the characterization studies on TiO_2/SiO_2 supported oxides are very limited. Fernandez et al. [69] performed a comparative study of small colloidal TiO_2 particles and 12 wt% TiO_2/SiO_2 supported oxides. The TEM micrographs show that both samples consist of very small particles (d<3 nm). A similar blueshift in the bandgap absorption edge of both samples was observed by UV–Vis spectroscopy, which is attributed to the quantum size effect. However, XPS analysis shows that a significant difference of −1.1 eV in the relaxation energy (the Auger parameter) with respect to the TiO_2 bulk oxide was observed for the TiO_2/SiO_2 supported oxides as compared to the difference of only −0.3 eV created by colloidal TiO_2 due to the particle size effect. The authors proposed that the SiO_2 support plays a more important role than the particle size and/or water content in decreasing the extra-atomic relaxation energy of the photohole, in agreement with the formation of Ti–O–Si bonds.

Raman studies of the dehydrated, dispersed TiO_2/SiO_2 supported oxides (TiO_2 loading <15 wt%) exhibit two bands at 950 and 1080 cm^{-1} [102], similar to that of TiO_2–SiO_2 mixed oxides, which is indicative of the formation of Ti–O–Si bonds. Furthermore, XPS analysis shows that the BE value of Ti $2p_{3/2}$ electrons for the dispersed TiO_2/SiO_2 supported oxides increases by about 0.8–1.9 eV [75] or 0.5–1.0 [102] as compared to pure TiO_2, while the BE value of O 1s electrons in Ti–O–Si is an intermediate value between Si–O–Si and Ti–O–Ti. These results strongly suggest the formation of Ti–O–Si bonds in TiO_2/SiO_2 supported oxides.

2.2.3. TiO_2/SiO_2 multilayers/thin films

TiO_2/SiO_2 multilayers/thin films can be regarded as one type of TiO_2/SiO_2 supported oxides. When TiO_2 layers are thin enough on the silica substrate, a highly dispersed titanium oxide species may be present. The physico-chemical nature of this extremely thin layer should be the same as that of the highly dispersed TiO_2/SiO_2 supported oxides. TiO_2/SiO_2 multilayers/thin films are often prepared by the deposition of evaporated titanium metal [103,104] or oxides [105,106] on the silica substrate, or by precipitation of hydrolyzed titanium alkoxide precursors [71,72]. Titania thin films with different morphology have been obtained by controlling preparation parameters, which is confirmed by small angle X-ray scattering (SAXS) and transmission electron microscopy (TEM) [71].

IR studies of TiO_2/SiO_2 multilayers/films show a band at 930 cm^{-1}, which was assigned to the vibration of Ti–O–Si bonds [105]. This band increases with decreasing the thickness of the TiO_2 multilayer films (down to 0.3 nm), while the crystallization of TiO_2 is lost. Also, with decreasing TiO_2 film thickness, an increase in surface hydration was observed [105], indicating an increase in the number of bonding defects and a similar surface behavior as the TiO_2/SiO_2 supported oxides.

Studies of the interface region of TiO_2/SiO_2 multilayers by electron energy loss spectroscopy (EELS) reveal that some EELS fine structures cannot be fitted to a combination of reference spectra of pure TiO_2 and SiO_2, but are representative of hybrid environments of Ti–O–Si. A zone of about 5 nm width at the interface was estimated to contribute to the presence of a TiO_2/SiO_2 solid solution with Ti–O–Si bonds [106].

The formation of Ti–O–Si bonds strongly modifies the electronic structure of the oxygen and titanium atoms at the interface of TiO_2/SiO_2 multilayers. At low Ti coverage, XPS analysis detected a new O 1s peak at 531.2 eV, which is between Si–O–Si (532.9 eV) and Ti–O–Ti (530.7 eV), suggesting the formation of Si–O–Ti bonds [103]. In addition, a significant blueshift in the bandgap edge of the supported TiO_2 thin films was observed by UV–Vis spectroscopy, which has been attributed to a combination of the size quantization effect and the substrate effect [103], with the substrate effect being more important [104].

2.2.4. Characterization of the molecular structure of the surface Ti atoms on SiO_2

Since the Ti atoms in TiO_2/SiO_2 supported oxides are located at the surface of silica, a higher Ti–OH concentration is expected due to a higher degree of coordinative unsaturation at the surface. The Ti–OH groups due to highly dispersed TiO_x species on the silica surface have been observed by FTIR and ^{1}H MAS NMR spectroscopy [77]. However, these hydroxyls are not stable and begin to dehydroxylate at a temperature of 180°C [77]. The molecular struc-

ture of the dispersed TiO_x species on silica in the hydrated state has been examined by EXAFS/XANES [8]. The pre-edge feature and the EXFAS data suggest that the Ti atoms are fivefold coordinated mononuclear and binuclear species with 2–3 Ti–OH hydroxyls. However, this assignment is quite questionable, and will be discussed later in Section 2.3.2.

Systematic investigation of the surface structure of dispersed TiO_2/SiO_2 supported oxides under hydrated and dehydrated conditions has recently been conducted by Gao et al. [102]. They employed in situ UV–Vis DRS and XANES spectroscopies to provide more reliable structural information. It was found that the surface structure of TiO_x species on silica is a strong function of environmental conditions as well as the TiO_2 loading. In the dehydrated state, 1.05 wt% TiO_2/SiO_2 is predominantly composed of isolated TiO_4 units (the LMCT band $\sim$47 600 cm^{-1}), 6.58 wt% TiO_2/SiO_2 of dimeric or one-dimensional polymerized TiO_4 units (the LMCT band $\sim$40 600 cm^{-1}), and 14.75 wt% TiO_2/SiO_2 of two-dimensional, polymerized TiO_5 units (the LMCT band $\sim$39 000 cm^{-1}).

Pronounced structural changes were observed upon hydration [102]. A Raman band appears at 940–960 cm^{-1}, which is most likely due to the Ti perturbed Si–OH. The adsorption of water molecules breaks the Ti–O–Si bridging bonds, resulting in the formation of Ti–OH hydroxyls as well as the Ti perturbed Si–OH. XANES analysis demonstrated that hydration appears to increase the average coordination number of the surface Ti cations by 1 for the dispersed TiO_2/SiO_2 supported oxides [102].

2.3. *Structural difference and similarity between titania–silica mixed and supported oxides*

2.3.1. *Comparison of various characterization data*

The most important spectroscopic features associated with the atomically mixed TiO_2–SiO_2 oxides and the highly dispersed TiO_2/SiO_2 supported oxides are summarized in Table 2. Characterization data on the relatively well-documented TS-1 (Ti-silicate) are shown for reference. The comparison between the characterization data on these materials could shed some light on understanding the behavior of Ti atoms in different local environments.

As shown in Table 2 XPS analysis of the three types of materials indicates that the BE value of the Ti $2p_{3/2}$ electrons significantly increases when connected with different silica matrices. This result can be explained in terms of the increase of the effective positive charge on the Ti atoms due to the Ti–O–Si linkages, as discussed previously. The large shift of the BE value of Ti $2p_{3/2}$ electrons ($\geq$1 eV) is usually associated with the isolated TiO_4 sites that possess maximum number of Ti–O–Si bonds per Ti atom.

In agreement with the XPS data, similar vibrational bands are observed on mixed and supported titania–silica oxides as well as TS-1, suggesting that these vibrations can only be safely associated in the presence of Ti–O–Si linkages. The assignment of the IR band at $\sim$960 cm^{-1} and its Raman counterpart at $\sim$960 cm^{-1} in Ti-silicalites has been discussed in detail in the literature. These are due to silica vibrations perturbed by the presence of Ti and are indicative of the formation of $Ti^{\delta+}$–$O^{\delta-}$–Si bonds [38,107]. The Raman band at 1080–1200 cm^{-1} has been assigned to the stretching modes of other Si–$O^{\delta-}$ bonds indirectly perturbed by the presence of Ti [107]. A more detailed assignment has been given by Deo et al. [38]. They assigned this band to the SiO_4 unit containing two non-bridging oxygens as in the case of some silicate glasses. Since EXAFS analysis shows that there are no [TiO_x] units sharing edges with [SiO_4] units [96] and Ti is connected to four [SiO_4] units in Ti-silicalite [108], the only possible presence of a SiO_4 unit with two non-bridging oxygens is in the structural unit of Ti–O–Si–O–Ti. However, there are no available techniques capable of detecting the presence of Ti–O–Si–O–Ti linkages. In fact, the Ti atoms that perturb the vibrational modes of the [SiO_4] units are not necessarily located in a tetrahedral environment, since the coordination changes due to the addition of NH_3 and H_2O cause only slight changes in the vibrational spectra [38,107].

The comparison of the UV–Vis results of the three types of materials indicates that titania–silica mixed and supported oxides at low Ti contents (<5%) predominantly possess isolated TiO_4 species (the LMCT band at 45 000–50 000 cm^{-1}). Nevertheless, the LMCT band of TS-1 is usually higher than these of titania–silica mixed and supported oxides, suggesting that isolated TiO_4 sites in titania–silica mixed and supported oxides even at low Ti contents are not

Table 2
Comparison of various characterization data on TS-1, TiO_2–SiO_2 mixed oxides and TiO_2/SiO_2 supported oxides

Techniques	TS-1	TiO_2–SiO_2 mixed oxides	TiO_2/SiO_2 supported oxides	Reference
XPS				
ΔBE (Ti $2p_{3/2}$)[a]	1.5	1.2–1.3 eV	0.8–1.9 eV	[65,67,75,126]
IR				
Ti–O–Si vibration	960 cm^{-1}	910–960 cm^{-1}	930 cm^{-1}	[85,105,107]
Raman	960 cm^{-1}	935–960 cm^{-1}	950 cm^{-1}	
Ti–O–Si vibration	1125 cm^{-1}	1100–1110 cm^{-1}	1080 cm^{-1}	[38,85,102]
UV–Vis				
LMCT peak (dehydrated)	45 000–50 000 cm^{-1}	40 900–45 000 cm^{-1}	39 000–47 900 cm^{-1}	[85,88,102]
XANES (dehydrated)[b]				
Pre-edge peak intensity	75%	58%	65%	[85,102]
Pre-edge peak position[c]	4969.7 eV	4969.7 eV	4969.5 eV	
EXAFS				
Ti–O bond length (average)	1.80–1.81 Å	1.81–1.82 Å	1.81 Å	[68,81,85,96]
Ti–O–Si bond angle	163°	159°	–	[108,115]

[a] ΔBE ($Ti2p_{3/2}$) corresponds to the increase of the BE in Ti–O–Si bonds as compared to Ti–O–Ti bonds.
[b] Samples with low Ti contents (<2 wt% TiO_2) are used for comparison.
[c] Pre-edge peak position given using first inflection point of Ti foil at 4966.0 eV.

unique, and a small amount of polymerized Ti species may also be present. The maximum LMCT band of titania–silica mixed and supported oxides redshifts with increasing Ti content [93,102], suggesting an increase in the polymerization degree of Ti atoms [102]. The maximum polymerization degree of Ti atoms is observed on the monolayerly dispersed TiO_2/SiO_2 supported oxides as extended two-dimensional, polymerized TiO_5 units. Moreover, UV–Vis results indicated that hydration increases the total number of Ti–O–Ti bonds (polymerization degree) of TiO_2/SiO_2 supported oxides at high loadings (>5 wt%TiO_2) [102]. Similarly, Klein et al. [93] also observed an increasing tendency for the formation of Ti–O–Ti bonds through hydration at higher Ti-contents in the mixed TiO_2–SiO_2 oxides.

2.3.2. *Are the structural assignments reasonable?*

Most of the structural information about titania–silica comes from Ti K-edge EXAFS/XANES studies. However, the fitted value of the coordination number from EXAFS data often shows a relatively large variation, even in the case of TS-1 (±0.5–0.6) [85,96], which gives rise to uncertainty in the prediction of the coordination number of the Ti atoms in the titania–silica system. Therefore, it is necessary to develop a reliable approach to verify the feasibility of structures proposed by EXAFS/XANES studies.

A general empirical relationship for relating the Ti^{4+}–O bond strength s_i to bond length R (Å) has been developed by Brown and Wu [109] based on the data from many Ti–O-containing compounds with Ti^{4+} cations in different environments:

$$s_i\,(\mathrm{vu}) = (R/1.806)^{-5.2} \quad (\mathrm{vu} = \text{valence unit}). \qquad (2)$$

According to the valence sum rule, the sum of each individual Ti–O bond valence relating to a Ti^{4+} site is:

$$\sum s_i\,(\mathrm{vu}) = 4.00 \pm 0.20\,\mathrm{vu}. \qquad (3)$$

This bond valence–bond length correlation can provide a more stringent constraint on the local environment around Ti in Ti-silicates, titanates and Ti–O-containing compounds. By using the Ti–O bond lengths derived from Ti K-edge EXAFS data, the valence states of Ti^{4+} cations in some compounds/

Table 3
Valence state of Ti^{4+} cation in various Ti–containing materials obtained from Ti–O bond lengths derived from Ti K-edge EXAFS data

	Ti–O bond length (Å)	Average Ti–O (Å)	Valence state $\sum s_i$ (vu)	Reference
6-Coordinated				
TiO_2 (anatase)	1.93×4, 1.98×2	1.95	4.04	[96]
TiO_2 (rutile)	1.95×4, 1.98×2	1.96	3.93	[96]
5-Coordinated				
$Na_4Ti_2Si_8O_{22}.4H_2O$	1.70×1, 1.96×4	1.91	3.98	[110]
$Rb_2Ti_4O_9$	1.65×1, 1.98×4	1.91	4.08	[111,112]
$Ti(OEt)_4$ and $Ti(OBu^n)_4$	1.80×3, 2.05×2	1.90	4.09	[114]
Ti–silicate/aluminosilicates	(1.67–1.70)×1, (1.94–1.95)×4	1.89	4.13–4.18	[113]
TiO_2/SiO_2 supported oxide (hydrated)	1.75×3, 1.86×1, 2.00×1	1.82	4.98(?)	[8]
4-Coordinated				
$Ni_{2.6}Ti_{0.7}O_4$	1.84×4	1.84	3.68	[111,112]
$Ti(OAm^t)_4$ and $Ti(OPr^i)_4$	1.80×4	1.80	4.07	[114]
TS-1	(1.80–1.81)×4	1.80–1.81	4.07–3.95	[94,96]
TiO_2/MCM-41 (dehydrated)	1.81×4	1.81	3.95	[115]
TiO_2–SiO_2 mixed oxide/glasses	(1.81–1.82)×4	1.81–1.82	3.95–3.84	[68,81]

oxides with different coordinations are calculated and shown in Table 3. The Ti^{4+} cations in the compounds/oxides listed there, possess a total valence state between 3.68 and 4.18 vu. The average Ti–O bond lengths for the different coordinations are 1.80–1.84 Å for fourfold, 1.89–1.91 Å for fivefold, and 1.95–1.96 Å for sixfold, as listed in Table 3. It should be mentioned that for fivefold coordinated compounds/oxides, it does not matter whether Ti is in square pyramidal [110,111–113] or in distorted trigonal bipyramidal coordinations [114], the valence state of Ti and the average Ti–O distance always fit into the expected range. Thus, it appears that the total valence state of a Ti^{4+} cation obtained from the Ti–O bond lengths and the average Ti–O bond length can be used to justify the local structure of the Ti atoms in various environments.

The valence states and the average bond lengths for TS-1 and the atomically mixed TiO_2–SiO_2 oxides are consistent with the standard set for a tetrahedral coordination. The Ti atoms in TS-1 are isolated as demonstrated by EXAFS experiment [96,108]. For atomically mixed TiO_2–SiO_2 oxides, although it is believed that the Ti atoms are also isolated, the experimental evidence seems insufficient since the Ti–Ti distances have not been reported in the literature.

The only exception to the valence sum rule in Table 3 is the result reported by Yoshida et al. [8] for the dispersed TiO_2/SiO_2 supported oxides in hydrated conditions. The valence state for a Ti^{4+} cation is calculated to be 4.98 vu, which is significantly out of the acceptable range. Moreover, the average Ti–O bond length is very short (1.82 Å), which is within the range of fourfold coordination instead of fivefold coordination. This discrepancy might be accounted for by the poor quality of the fitting values and incorrect assignment of the Ti coordination. In contrast, a well-performed EXAFS study by Maschmeyer et al. [115] on the TiO_2/MCM-41 (mesoporous silica) supported oxides indicates that the valence state and the average bond-length of Ti^{4+} cations are in excellent agreement with the standard set for a tetrahedral coordination. Their EXAFS experiment shows that the fourfold coordinated Ti atoms are located at the wall of mesopores, and act as the active centers for the epoxidation reaction.

The pre-edge features in XANES spectra have been regarded as a supplementary evidence for the presence of certain coordination geometry based on the comparison with the model compounds. Furthermore, the absolute position and intensity of pre-edge peak have been considered to be the key factors in determining the coordination number of Ti [111,112,113]. The pre-

edge features with the highest intensity at the lowest energy correspond to Ti in tetrahedral sites and the opposite pattern holds for Ti in octahedral sites. As listed in Table 2, the pre-edge position is about the same for the three different types of materials with similar low Ti contents, however, the pre-edge intensity is the highest for TS-1. The slightly lower pre-edge intensity for titania–silica mixed and supported oxides implies that their average coordination number and/or the distortion of coordination geometry are slightly higher than that of TS-1.

It is concluded for both atomically mixed TiO_2–SiO_2 oxides and molecularly dispersed TiO_2/SiO_2 supported oxides that at low Ti contents, the Ti atoms predominantly reside in isolated tetrahedral sites with possibly a small amount of higher coordination Ti sites. The isolated TiO_4 sites are coordinatively unsaturated and are subject to change upon hydration. Polymerization of Ti atoms occurs at high Ti contents, which results in an increase in the average coordination number of Ti atoms.

2.3.3. *Location of the Ti atoms*

The location of the Ti atoms is a very important issue because catalysis only takes place at the surface. For TiO_2/SiO_2 supported oxides, there is no doubt that the Ti atoms are mostly located on the outer surface of the silica support. For TiO_2–SiO_2 mixed oxides, however, not all the Ti sites are accessible [12]. As will be shown later, TiO_2–SiO_2 mixed oxides not only possess Lewis acidity but also generate new Brønsted acid sites. The location of these Ti atoms should be on the surface of micro, meso- or macro-pores that are accessible to the reactants or probe molecules. Since the surface Ti sites are potential adsorption sites for some reactants such as alcohols [19,116] and for probe molecules such as NH_3 and pyridine [12,19], it is possible to employ some selective adsorbing molecules to measure the number of surface Ti atoms. Evidently, the size and adsorption selectivity of the probe molecules are crucial for determining the right number of surface Ti atoms. However, up to now, no suitable method has been established due to the incomplete understanding of the structure–adsorption relationships between the mixed oxides and the probe molecules.

As discussed previously, the maximum Si/Ti atomic ratio for the atomically mixed TiO_2–SiO_2 is ca. 7.5, which corresponds to 3–4 Ti atoms/nm^2 if we consider that all the Ti atoms are located around the surface with an average surface area of 300–400 m^2/g. It is possible that most of the Ti atoms in the atomically mixed TiO_2–SiO_2 oxides reside near the surface, since the maximum loading for the molecularly dispersed TiO_2/SiO_2 supported oxides is ca. 4 Ti atoms/nm^2. Liu et al. [12] reported that a large fraction of Ti atoms in the TiO_2–SiO_2 mixed oxides with Si/Ti molar ratio of 8.2 is located around the surface (corresponding to ca. 2.6 Ti atoms/nm^2).

Mukhopadhyay and Garofalini [67] have pointed out that a surface rich in Ti is energetically less favorable than rich in Si. XPS and XANES studies of TiO_2–SiO_2 mixed oxide prepared by coprecipitation reveal that the surface is enriched in Si and the degree of enrichment increases with Ti content [65]. As will be discussed later (Section 3.2.2), the acidity studies by ammonia and pyridine adsorption demonstrate that the surface enrichment of Ti or Si is a strong function of preparation procedures and chemical compositions. In general, TiO_2–SiO_2 mixed oxides with a high Ti content exhibit surface enrichment of Si. In fact, the significantly higher surface area of TiO_2–SiO_2 mixed oxides (even with a very low SiO_2 content) than the surface area of pure TiO_2 may also be accounted for by the surface enrichment of Si atoms that locate near the surface to stabilize the material from sintering.

It is interesting to note that no matter what the preparation methods (mixed oxides or supported oxides) or chemical compositions are employed, the Ti/Si atomic ratios obtained by XPS experiments are often lower than the corresponding calculated bulk ratios [28,65,74,75,102]. It is hard to believe that the surface enrichment of Si that might occur in mixed oxides could also occur on the supported oxides where the highly dispersed TiO_x species are supposed to anchor on the silica surface via its outermost layer of hydroxyls. This implies that either the Ti atoms are located on the surface of inside channels or pores of silica that is out of the XPS detection range, or there might be some type of experimental error that underestimates the concentration of Ti versus Si. Therefore, XPS analysis may not be a suitable technique for providing reliable quantitative information about the surface enrichment of Ti or Si.

3. Structure–property relationships for titania–silica as catalysts

3.1. Electronic properties and photocatalysis

3.1.1. Quantum-size effect and support effect

Silica has been widely used as a substrate or matrix to disperse and stabilize nano-sized TiO_2 particles [1,3,5,6,7,103,117]. The UV absorption edge, or optical band-gap, is a strong function of the TiO_2 particle size with diameters less than 4 nm. These small particles consist of a few hundred TiO_2 molecules [98], which are believed to exhibit the well-known quantum-size effect. The quantum-size effect of TiO_2 on/in SiO_2 has been repeatedly reported [1,74,103,117]. The study of the TiO_2/SiO_2 multilayer films by Nakayama et al. [117] showed that the TiO_2 size change even in one dimension also shows the quantum-size effect. Nakayama et al. found that the optical energy gap E_g remains constant until the thickness of TiO_2 films on SiO_2 are reduced to less than 2 nm, then E_g increases as the film thickness further decreases.

As discussed previously, the Ti–O–Si bonds strongly modify the electronic structure of the Ti atoms in both titania–silica mixed and supported oxides, and increase the effective positive charge on the Ti atoms. As pointed out by Lassaletta et al. [103,104], the increase in the band-gap energy could be attributed to a combination of the quantum-size effect and the interface interaction due to the support effect, with the support effect probably being the most important.

TiO_2 (anatase) has a band-gap of ca. 3.3 eV, while the band-gap for titania–silica can be increased up to ~4.1 eV due to the above two effects [103]. An increase in the band-gap of the nano-sized TiO_2 particles has been ascribed to an elevation of the conduction band edge as well as the lowering of the valence band edge [98,118]. Thus, the electronic properties are changed due to the increased band-gap energy. The oxidizing potential of the photon generated holes (h^+) and the reducing potential of the photon generated electrons (e^-) will increase with increasing band-gap, as shown in Scheme 1.

Therefore, the nano-sized TiO_2 particles in or on SiO_2 possess high photo-oxidation as well as photo-reduction capabilities.

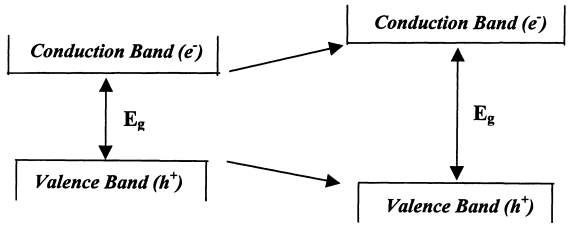

Scheme 1.

3.1.2. Photocatalysis

Since the nanosized TiO_2 particles possess a larger band-gap with a higher photo-oxidation capability, the strong oxidizing potential of the photogenerated holes has made titania–silica one of the most attractive photocatalysts for oxidation reactions. For example, TiO_2–SiO_2 gel has been used for decontamination of aquatic environment [1]. The rate of photodecomposition of organic pollutants was reported to increase as the TiO_2 particle size decreased, which is in agreement with the increasing oxidation potential of the oxidizing holes.

In addition to the improved oxidizing abilities, some synergism between the TiO_2 and SiO_2 phases has been noticed by Anderson and Bard [5,6]. They found that TiO_2–SiO_2 gel shows a higher photodecomposition rate of rhodamine-6G (R-6G) as compared to TiO_2 (P-25) [5]. Since R-6G adsorbs on SiO_2 sites, but not on TiO_2, the presence of an adsorbent (SiO_2) was considered to promote the efficiency by increasing the concentration of R-6G near the TiO_2 sites relative to the solution concentration of R-6G. They suggest that the photogenerated intermediate oxidants on the TiO_2 sites, such as hydroxyl radical ($HO^{\bullet}$) or species from reduction of O_2 ($HO_2^{\bullet}$), must diffuse and react with R-6G on the SiO_2 sites. Similar synergy mechanism, but with the organic molecules being activated in the TiO_2–SiO_2 region, has been suggested to explain the increased activity of the photocatalytic decomposition of phenol on TiO_2–SiO_2 gel [6].

The strong reduction potential of nano-sized TiO_2 in sol–gel prepared TiO_2–SiO_2 mixed oxides has been observed by Inoue et al. [3]. TiO_2–SiO_2 mixed oxides shows higher activities for photocatalytic reduction of CO_2 to formate, methane and ethylene compared to pure TiO_2. The authors demonstrated that the activities (i.e., quantum efficiencies) of TiO_2–SiO_2 mixed

oxides increase with decreasing size of the TiO_2 microcrystals.

However, the above results would have made more sense if the total effective surface area of the nano-sized TiO_2 particles could be known. A method based on the selective adsorption of isopropanol for measuring the effective surface area of titania on silica, has been suggested by Biaglow et al. [116]. They found that the total effective titania surface area measured on titania–silica could be three times higher than that of pure TiO_2. This fact implies that the increased surface area due to the decreased particle size may also contribute to the increased photocatalytic activity. Therefore, it is not quite clear from the above results whether the enhanced photocatalytic activity is due to the increased effective TiO_2 surface area or due to the increased oxidizing or reducing potentials.

3.2. Acidic properties and acid catalysis

3.2.1. Coordination geometry and generation of new Brønsted acid sites

Titania–silica has been employed for a number of acid catalyzed reactions such as isomerization and dehydration, see Table 1. The acidic properties of titania–silica are quite different from that of either pure titania or pure silica, since pure titania only possesses Lewis acidity while silica has neither Brønsted nor Lewis acidity. However, new Brønsted acid sites are created when titania and silica form Ti–O–Si chemical bonds [12,18,19,119,120].

Several models have been proposed to explain the generation of the new acid sites [118,119,121]. A charge imbalance localized at the Ti–O–Si bond has been attributed to the generation of new acid sites [119,121]. Tanabe et al. [121] first proposed a model for mixed binary oxides based on two hypotheses. According to their hypotheses, the coordination numbers of Ti and Si are maintained at 6 and 4, respectively, as in the pure oxides. In addition, oxygen assumes the coordination number of the major component oxide, i.e., in Ti-rich mixed oxides, the coordination number for all oxygens is 3, while in Si-rich mixed oxides, the coordination number is 2. Therefore, in Ti-rich mixed oxides, Si is the acid site and an excess of the positive charge of +4/3 distributed on four Si–O bonds is produced and assumed to generate Lewis acidity. While in Ti-rich mixed oxides, Ti is the acid site and an excess of the negative charge of -2 distributed on six Ti–O bonds is produced and assumed to generate Brønsted acidity. However, Tanabe's model is not consistent with more recent structural characterization data. As described previously, in Si-rich mixed oxides, the coordination number of the Ti atoms that substitute into the silica network is 4, not 6. Moreover, the Ti-rich mixed oxides show a substantial amount of new Brønsted acid sites that cannot be explained by this model [12,19].

Nakabayashi et al. [118] explained the generation of new and strong Lewis acid sites on finely divided pure TiO_2 by the quantum-size effect. They demonstrated that the acid strength of TiO_2 particles increases as the particle size decreases, which is explained in terms of the lowering of the valence band edge associated with the enlarged bandgap due to the quantum-size effect. However, this effect could not account for the formation of new Brønsted acid sites in TiO_2–SiO_2 mixed oxides [120], and Nakabayashi has to attribute the new Brønsted acidity also to the presence of Ti–O–Si bonds.

Kataoka and Dumesic [119] proposed a model based on the studies of silica-supported metal oxides by pyridine adsorption with infrared spectroscopy. They found that the strength of Brønsted acidity on 1 wt% TiO_2/SiO_2 is rather weak. When the sample was evacuated at 420 K, only Lewis acid sites were detected. Brønsted acid sites were generated when water vapor was introduced at room temperature. When TiO_2/SiO_2 was reduced, no Brønsted acidity was observed even in the presence of water vapor. According to Pauling's electrostatic valence rule, they stated that the degree of undersaturation for surface oxygens is dependent only on the valence and the coordination of the cations, and the terminal hydroxyls can never be acidic. The Brønsted acid sites are generated on M–O–Si bridges to compensate for the undersaturated bridging oxygen as in the case of silica–alumina. According to this model, Ti in tetrahedral coordination is not expected to generate Brønsted acidity because the undersaturation of oxygen in Ti–O–Si bond is zero. However, when octahedral coordinated Ti is produced in the presence of water vapor, an undersaturation of 0.33 valence unit (vu) for Ti–O–Si bridging oxygen is resulted, and a proton is needed to saturate such oxygen, therefore, Brønsted acidity is generated. With this model, the

undersaturation for Ti–O–Si bridging oxygen with Ti in pentahedral coordination is estimated to be 0.2 v.u., and Brønsted acidity should also be observed. Evidently, the Brønsted acidity on titania–silica is expected to be rather weak due to the change of coordination geometry of Ti upon dehydration as well as the poor stability of hydroxyls associated with Ti.

In both Tanabe's and Kataoka and Dumesic's model, the difference in coordination geometry of Ti from Si in Ti–O–Si bond plays a vital role in causing a charge imbalance to generate Brønsted acid sites. Kataoka and Dumesic's model seems more consistent with the experimental results. This model predicts that:

1. Brønsted acid sites are associated with Ti–O–Si bridges where the Ti atoms reside *not* in tetrahedral sites but in pentahedral or octahedral sites, regardless of composition;
2. the coordination change of the Ti atoms upon hydration will generate weak Brønsted acid sites.

These predictions are quite consistent with recent results by several research groups [12,59,80]. Liu et al. [12] reported that the Brønsted acidity in atomically mixed TiO_2–SiO_2 oxides is correlated with the non-tetrahedral sites. In addition, surface hydroxylation is crucial to the presence of Brønsted acidity [19,59]. In this model, the bridging Ti–OH–Si hydroxyls are supposed to be the Brønsted acid sites, in line with the generation of Brønsted acid sites in alumina–silica zeolites.

More recently, Liu et al. [12] modified Tanabe's model to explain the generation of Brønsted acid sites in Ti-rich mixed oxides. They proposed that the positive charge (+4/3) on Si is balanced by a hydroxyl group on Si, thus producing Brønsted acidity. In contrast, Contescu et al. [59] proposed that the acidic hydroxyl might be located on a titanium surface ion. Although it is widely accepted that the Brønsted acid sites are associated with the Ti–O–Si bridges, however, the exact location of the proton is still open to question.

3.2.2. *Acidic properties and isomerization/dehydration reactions*

To understand the acidity characteristics of titania–silica better, the relationship between the acidic properties (e.g., the strength, the amount and the type of acid sites) and the acid catalyzed isomerization and dehydration reactions will be discussed below. Because of the great concern about the possible residual contaminants of sulfate and/or alkali (Na^+) that might significantly modify the acidity of the catalyst, the acidic characterization results obtained from the samples prepared from precursors such as titanyl oxysulfate and sodium/potassium silicates will not be considered in this paper.

The acidity (in terms of both density and strength) of solid catalysts is usually measured by TPD of ammonia or pyridine, IR studies of ammonia or pyridine adsorption, and amine titration with Hammett color indicators. The experimental determination of acidity is a complex issue since the coordination geometry of Ti that determines the acidity of mixed oxides is different under different experimental conditions. The amine titration with Hammett indicators in non-aqueous solvents at room temperature measures the ability of oxides to protonate various basic indicators. The acidity measured in this way cannot reflect well the acidity under specific reaction conditions, therefore, this type of acidity measurement will not be cited here. TPD and IR studies of ammonia/pyridine adsorption can measure acidity under conditions closer to reaction conditions and can provide valuable information about the acidity profile of mixed oxides when related to the acid catalyzed reactions, and these results will be discussed here. The 1-butene isomerization and alcohol dehydration reactions occur at mild temperatures and are frequently employed to probe the acidic properties of solid surface, see Table 1. These reactions can be regarded as ''catalytic acidity'' measures and can provide better insight for understanding titania–silica as a solid acid catalyst. Moreover, it was found that the isomerization activity is greatly enhanced due to the presence of Brønsted acid sites. Thus, isomerization is considered as a selective chemical probe reaction for Brønsted acidity [12,14,17,19,59,120]. On the other hand, the alcohol dehydration is catalyzed by both Lewis and Brønsted acid sites and is proportional to the total number of acid sites on the catalyst, and therefore, it is considered as a measure for total acidity [19,114].

The acidic properties of TiO_2–SiO_2 mixed oxides depend largely on the preparation method, synthesis condition and chemical composition, which are in turn

related to the Ti–O–Si connectivities, the degree of surface hydroxylation and TiO_2 particle size as discussed above [12,13,19,59]. The acid strength, when evaluated by TPD and IR experiments of ammonia adsorption, shows a decreasing trend with increasing Si content [12]. The surface density (per surface area) of Brønsted acid sites is generally seen to be the highest in Ti-rich mixed oxides [12,19,28]. The surface density of total acid sites on TiO_2–SiO_2 mixed oxides, both the Lewis and Brønsted acid sites, when measured with ammonia or pyridine adsorption, generally decreases with increasing Si content over the whole composition range [12,13,19,28], as shown in Fig. 1. The decreased total acid sites with increasing Si content can be accounted for by the decreased surface density of the exposed Ti atoms. It is worthwhile to point out that the two curves of the total acidity (per surface area) shown in Fig. 1 are different, which may result from the different preparation procedures and acidity measurement procedures. The first curve obtained from [19] shows a quite linear relationship of the total acid sites with the Ti mol% up to high Ti content of 92 mol% Ti. While the second curve obtained from [12] shows a sharp increase of the total acid sites with increasing Ti concentration up to ~18 mol% TiO_2, and the total acid sites keeps almost constant with only a slight increase up to TiO_2 content of 85 mol%. The sharp increase at low Ti contents on the second curve might be explained by the high fraction of Ti atoms located on the surface [12]. As the Ti content increases, the fraction of the exposed Ti atoms appears to decrease while keeping the surface density of the exposed Ti atoms almost constant. In addition, both data sets show that the density of acid sites on pure TiO_2 is higher than the end point of the curve when extrapolated from the data of TiO_2–SiO_2 mixed oxides with different chemical compositions, suggesting that the surface of the mixed oxides at a high Ti content is rich in Si. These acidity studies show that the surface of Si-rich mixed oxides might be rich in Ti depending on the preparation procedures, whereas the surface of Ti–rich mixed oxides is most likely rich in Si. In conclusion, the surface enrichment of Ti or Si is a strong function of preparation procedure and chemical composition.

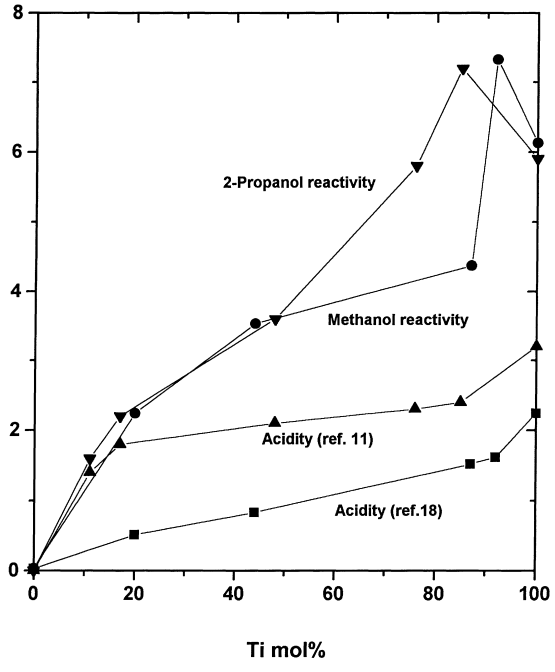

Fig. 1. Acidity and alcohol dehydration reactivities as a function of Ti concentration for TiO_2–SiO_2 mixed oxides. (Acidity (10^6 mol/m^2) data are adapted from [12,19], methanol dehydration reactivity (10^{-2} μmol/min m^2) from [19], and 2-propanol reactivity (10^{-1} percentage of 2-propanol reacted) from [12].)

Since butene isomerization and alcohol dehydration occur at moderate temperatures (423–523 K), it is expected that the catalyst surface is partially hydrated. This is supported by FTIR experiments that demonstrate that a large number of surface hydroxyls are present under reaction conditions [17]. Consequently, the reaction activity will be determined by the type, density and strength of surface acid sites present under the specific reaction condition.

The isomerization of 1-butene on TiO_2–SiO_2 mixed oxides has been reported to be acid-catalyzed, proceeding via butyl-carbonium ion as the intermediate [12,15]. The enhanced isomerization activity is attributed to the Brønsted acidity generated in the mixed oxides [12,14,59]. Contescu et al. [17,59] found a Brønsted-type linear correlation between the specific isomerization rates and the surface density of one particular type of site identified in the pK spectrum of the hydrous oxide surface. They concluded that both quantity and quality of Brønsted acid sites affect the overall catalytic performance. This conclusion is also supported by results obtained by Liu et al. [12]. Their results show that although the density of acid sites in Ti-rich mixed oxides is about two times higher

than in Si-rich mixed oxides (more than 80% of the acid sites on either Ti-rich or Si-rich mixed oxides is of Brønsted type), the specific rate of butene isomerization in Ti-rich mixed oxides is about six times higher than in Si-rich mixed oxides. Thus, the lower acid strength in silica-rich mixed oxides is responsible for the much lower isomerization acidity as compared to Ti-rich mixed oxides. The fact that the highest specific isomerization rate is generally located around 70–90 mol% TiO_2–SiO_2 mixed oxides [12–15] also demonstrates that in butene isomerization reaction the quality of Brønsted acid sites (acid strength) may also play a very important role in addition to the quantity of Brønsted acid sites. Unfortunately, the isomerization reaction has not yet been applied for the investigation of the acidic properties of TiO_2/SiO_2 supported oxides, which could provide some interesting comparative implications.

Alcohol dehydration provides additional information about the acidic properties of titania–silica. Results re-interpreted from methanol dehydration on TiO_2–SiO_2 mixed oxides [19] show that the specific reactivity generally increases with the surface density of acid sites, however, the increment is higher than the increment of the density of acid sites. Moreover, a maximum is observed in the Ti-rich mixed oxides, see Fig. 1. Results from isopropanol dehydration [12] also show a similar trend when the isopropanol dehydration reactivity is interpreted as the percentage of isopropanol molecules converted to propene. As discussed previously, the increased acid strength with increasing Ti content might partially contribute to the increased reactivity. However, this interpretation cannot explain the highest specific reactivity located around 80–90 mol% Ti, which is similar to the isomerization reaction on TiO_2–SiO_2 mixed oxides. This result might also suggest that the Brønsted acid sites are more effective than Lewis acid sites for alcohol dehydration since the surface density of Brønsted acid sites is generally seen to be the highest in Ti-rich mixed oxides [12,19,28].

Isopropanol dehydration has been applied to dispersed TiO_2/SiO_2 supported oxides by Biaglow et al. [116]. They tried to develop a method for measuring the titania surface area on TiO_2/SiO_2 supported oxides based on the selective adsorption of isopropanol. The percentage of isopropanol reacted on TiO_2/SiO_2 supported oxides is notably higher than pure TiO_2, which suggests that some Brønsted acid sites are present on the supported oxides during isopropanol dehydration. Unfortunately, the acidity studies for TiO_2/SiO_2 supported oxides are far less than the corresponding studies on TiO_2–SiO_2 mixed oxides, which prevent us from fully understanding the surface properties of dispersed TiO_2/SiO_2 supported oxides.

3.3. Local structure of Ti and epoxidation/oxidation reactions

3.3.1. Epoxidation/oxidation with hydrogen peroxide/alkyl hydroperoxides

Titania–silica mixed and supported oxides are effective catalysts for epoxidation and selective oxidation reactions using peroxides as oxidants, as shown in Table 1. For crystalline Ti-silicalites such as TS–1, the active sites are assumed to be the isolated tetrahedral TiO_4 units substituted in the framework [122], proceeding via titanium peroxocompounds as the reaction intermediate. The epoxidation mechanism involves no change in the oxidation state of Ti^{4+} cations [32]. The selective oxidation of saturated hydrocarbons with hydrogen peroxide on TS-1 also involves no change in the oxidation state of Ti cations, but possibly undergoes a radical type mechanism [22,122].

Titanium silicalites are superior to titania–silica mixed and supported oxides in epoxidation of lower olefins by hydrogen peroxide, but limited sterically to relatively small reactants that are capable of penetrating into the narrow channels where most active sites are located [22,31,122]. Recent studies by Hutter et al. [25,31] show that mesoporous TiO_2–SiO_2 mixed oxides are promising catalysts for epoxidation of bulky reactants such as cyclododecane, norbornene and α-isophorone. Their results indicate that when Ti is well-dispersed in the silica matrix with mesoporous structure, a high epoxidation activity is possible with some bulky reactants. Meanwhile Klein et al. [30,34] reported that amorphous microporous TiO_2–SiO_2 mixed oxides used for epoxidation of olefins with TBHP exhibit catalytic properties comparable to those of the crystalline Ti-silicalites. Moreover, the highly dispersed titanium oxide on amorphous silica and MCM-41 also demonstrate excellent catalytic activity in epoxidation of olefins by alkyl hydroperoxides [25,31,115].

Since the epoxidation reactions are usually carried out at low temperatures (323–363 K), polar solvents, particularly alcohols and water, greatly retard the reaction by competing for the active coordination sites [33]. The epoxidation of α-isophorone by TBHP with mesoporous TiO_2–SiO_2 aerogels [25] shows that the selectivity and reactivity of α-isophorone are markedly influenced by the solvent polarity. Polar solvents cause a significant drop in the activity by hindering the formation of the titanium–peroxide complex and the advance of the hydrophobic olefin to the active sites, and no activity was observed in water [25].

Extensive investigation has reached the conclusion that the major difference between crystalline Ti-silicalites and amorphous TiO_2–SiO_2 mixed oxides is that Ti-silicalites can utilize hydrogen peroxide as oxidant while the mixed oxides are only effective when using organic hydroperoxides, which is attributed to the much higher hydrophilicity as a result of a large number of surface hydroxyl groups on TiO_2–SiO_2 mixed oxides [22,26,30,38]. For example, due to the hydrophobic nature of TS-1 micropores (∼0.6 nm in diameter), H_2O is believed to be screened out from the cavities thus protecting the Ti sites from deactivation by H_2O [26,123].

The catalytic activity of olefins epoxidation with alkyl hydroperoxide on TiO_2–SiO_2 mixed oxides has been strongly correlated with the fraction of the Ti atoms in tetrahedral sites [26,28,30], or with the Ti–O–Si connectivity that is characteristic of Ti dispersion in the silica matrix [24]. The key factors determining the activity and selectivity of TiO_2–SiO_2 mixed oxides prepared by sol–gel method are assumed to be the morphology (surface area and pore size) and the relative proportions of Ti–O–Si to Ti–O–Ti bonds [31].

The highly dispersed TiO_2/SiO_2 supported oxides (<4%Ti) have been reported early by Sheldon [32,33] to be very effective for olefins epoxidation with alkyl hydroperoxides. The formation of Ti–O–Si bonds is crucial as demonstrated by the much lower activities of TiO_2 supported on other oxides and the physical mixture of TiO_2 and SiO_2 [33]. Sheldon suggested that the active sites are the isolated monomeric titanyl $(SiO)_2Ti{=}O$ groups. However, there is no experimental evidence to support the presence of Ti=O bonds on the silica surface. A recent report [115] shows that TiO_2 supported on mesoporous silica MCM-41 molecular sieve is highly active and selective for epoxidation of alkenes by TBPH. XANES/EXAFS studies demonstrated that all Ti atoms are isolated and located on the wall of MCM-41 mesopores. Interestingly, the coordination of these Ti atoms is fourfold after calcination, but changed to sixfold during the epoxidation reaction. This study strongly suggests that the surface active Ti centers on TiO_2/SiO_2 supported oxides for epoxidation reactions might also be isolated tetrahedral sites with four similar Ti–O bonds instead of $(SiO)_2Ti{=}O$.

Despite different reactants used in epoxidation reactions, which is largely dependent on the morphology (surface area and pore size) and surface properties (hydrophobicity) of catalysts, the high epoxidation reactivities on Ti-silicalites, titania–silica mixed and supported oxides strongly suggest that a structural similarity exists between the active sites on these different types of catalysts, i.e., isolated TiO_4 sites.

3.3.2. Redox ability and oxidation reactions

The redox properties of titania–silica are much less studied due to the low oxidation potential of Ti(IV) cations relative to some other transitional metal cations such as V(V), Mo(VI), Cr(VI), etc. The reduction of pure TiO_2 is difficult, since only a very small amount of surface Ti^{4+} cations can be reduced to Ti^{3+} cations as detected by CO adsorption but not by XPS experiment [124]. The reducibility of 7 wt% TiO_2/SiO_2 supported oxides has also been examined by CO adsorption and XPS experiments [74]. A small amount of the surface reduced Ti^{3+} cations was detected by both CO adsorption and XPS measurement after hydrogen reduction. However, the authors did not provide further information about whether the oxidation potential of the Ti(IV) cations on TiO_2/SiO_2 supported oxides is different from that of pure TiO_2.

An interesting phenomenon was observed with dispersed TiO_2/SiO_2 supported oxides during methanol oxidation [36,38,102]. Methanol oxidation is known as a chemical probe to distinguish between acid sites and redox sites [38]. For pure TiO_2, the surface Lewis acid sites result in almost complete production of dimethyl ether (the high coverage of the methoxy intermediate on TiO_2 may also contribute to the high selectivity of dimethyl ether). However, for the dispersed TiO_2/SiO_2 supported oxides, a high selectivity (≥94%) to the redox products (formalde-

hyde and methyl formate) was obtained, demonstrating that the redox property of surface TiO_x species on silica plays a key role. The decreased dehydration ability (formation of dimethyl ether) relative to the redox ability (formation of formaldehyde and methyl formate) suggests an increased oxidizing potential and a decreased acidity of the Ti cations when dispersed on the silica support. The increased oxidizing potential of the Ti(IV) cations, due to the formation of Ti–O–Si bonds, is also reflected by the increased BE value of Ti $2p_{3/2}$ and the higher LMCT transitions of the Ti atoms in the dispersed TiO_2/SiO_2 catalysts [102]. Similarly, methanol oxidation on Ti-silicalites also gives rise to a high selectivity of the redox products [38], indicating that the Ti^{4+} cations with Ti–O–Si linkages serve as the redox sites.

Furthermore, the highest specific catalytic activity of the dispersed TiO_2/SiO_2 supported oxides for methanol oxidation was observed at the lowest loading of 1.05 wt% TiO_2/SiO_2, which is dominated by the isolated TiO_4 sites [102]. The observation of the surface Ti-methoxy species resulting from the breaking of the Ti–O–Si bridging bonds by Raman and UV–Vis–NIR spectroscopy strongly supports the conclusion that methanol oxidation involves participation of Ti–O–Si bonds. The isolated TiO_4 sites provide the maximum number of Ti–O–Si bonds and, consequently, exhibit the highest specific activity for methanol oxidation. Polymerization of the surface Ti atoms on SiO_2 decreases the fraction of Ti–O–Si bonds and, thus, significantly decreases the activity of the Ti sites. This is in agreement with the activity pattern of the TiO_2–SiO_2 mixed oxides for liquid phase olefin epoxidation with alkyl hydroperoxide where the activity has been correlated with the Ti–O–Si connectivity or the relative proportions of Ti–O–Si to Ti–O–Ti bonds [24,31].

Contradictory results have been obtained for CO oxidation on TiO_2–SiO_2 mixed oxides [125]. The CO oxidation activity decreases with increasing Ti content, and pure TiO_2 shows the highest activity. This contradiction to the above reactions may be due to the different active sites needed for CO oxidation. However, on the basis of the quantum-size effect, the authors proposed that the increased energy gap between the lowest unoccupied molecular orbital (LUMO) and the highest occupied molecular orbital (HOMO) is responsible for the decreased redox ability. Unfortunately, when Ti is substituted into the silica network as an isolated TiO_4 unit, no corresponding theoretical study has been done to determine how the molecular orbital changes. It seems inappropriate to apply the band-gap theory to the isolated TiO_4 unit with localized Ti–O–Si bonds. As indicated by UV–Vis spectra, the charge transfer O→Ti(IV) occurs at the highest energy for the isolated TiO_4 unit in the silica network, which indicates some contributions from surrounding Si(IV) with a higher electronegativity. The electron-accepting ability (affinity) of Ti(IV) in Ti–O–Si bonds should be higher than in Ti–O–Ti bonds, in agreement with the increased BE value of Ti 2p as compared to pure TiO_2.

It is known that during reactions the coordination geometry of Ti may change from fourfold to five or sixfold coordination as in the case of the epoxidation reactions [115]. Consequently, the electron affinity of Ti is subject to change upon the coordination geometry generated during reactions, similar to the generation of new Brønsted acid sites upon hydration [119]. It is suggested that the oxidation potential of Ti(IV) is more likely related to its reaction intermediates formed during reactions than its initial states. In other words, the redox ability of Ti(IV) is dependent on the specific reaction environment. Therefore, the in situ investigation of the coordination geometry and the oxidation potential of Ti(IV) atoms during reactions is crucial for fully understanding the redox properties as well as the reactivity properties of titania–silica in oxidation reactions.

4. Summary

Titania–silica materials represent a novel class of catalysts and have been widely applied in photocatalysis, acid catalysis and oxidation catalysis. The intimate interaction of TiO_2 and SiO_2 has been shown to result in new structural characteristics and physicochemical/reactivity properties. The degree of interaction, in other words, the homogeneity or dispersion when TiO_2 is mixed with or supported on SiO_2, largely depends on the preparation methods and synthesis conditions. Also, the surface enrichment of either Ti or Si in TiO_2–SiO_2 mixed oxides has been shown to depend on the preparation conditions and chemical compositions.

Significant improvement in the fundamental understanding of the structural characteristics of titania–silica has been realized in recent years through the use of many advanced techniques. Some characterization techniques such as XPS, IR and Raman spectroscopies can provide information about the formation of chemically bonded Ti–O–Si linkages, which might be indirectly associated with the local structure of the Ti atoms. EXAFS/XANES spectroscopy is a powerful tool to investigate the local structure of Ti in titania–silica materials, however, the uncertainty in the fitting parameters is of great concern. The combined results from all these characterization techniques strongly suggest that at low Ti contents, both the atomically mixed TiO_2–SiO_2 oxides and molecularly dispersed TiO_2/SiO_2 oxides possess predominantly isolated TiO_4 sites. The difference in structural characteristics of titania–silica mixed and supported oxides may just be a matter of the degree of exposure, with TiO_2–SiO_2 mixed oxides having some of the Ti atoms located in the silica matrix.

The physico-chemical/reactivity properties of titania–silica are a strong function of the structural characteristics. New Brønsted acid sites are generated by the charge imbalance on Ti–O–Si bond due to the difference in coordination geometries of Ti and Si. The new Brønsted acid sites seem more effective for isomerization and dehydration reactions. The reactivities of epoxidation/oxidation reactions have been related to the exposed isolated TiO_4 sites as well as the fraction of Ti–O–Si bonds. The structural characteristics under specific conditions are crucial for understanding the catalytic behavior of titania–silica in a reaction, since the coordination geometry and the physico-chemical properties of Ti changes in the reaction. Therefore, future experiments should focus on the in situ investigation of the coordination and oxidation states of the Ti atoms in titania–silica so as to develop a fundamental understanding about the catalysis and chemistry of this interesting and important catalytic material.

Acknowledgements

The authors would like to thank Dr. Simon R. Bare for his helpful suggestions and comments on the original paper. This work was financially supported by the US National Science Foundation Grant CTS-9417981.

References

[1] G. Dagan, S. Sampath, O. Lev, Chem. Mater. 7 (1995) 446.
[2] R.W. Matthews, J. Catal. 113 (1988) 549.
[3] H. Inoue, T. Matsuyama, B. Liu, T. Sakata, H. Mori, H. Yoneyama, Chem. Lett. (1994) 653.
[4] M. Anpo, K. Chiba, J. Mol. Catal. 74 (1992) 207.
[5] C. Anderson, A.J. Bard, J. Phys. Chem. 99 (1995) 9882.
[6] C. Anderson, A.J. Bard, J. Phys. Chem. B 101 (1997) 2611.
[7] X. Fu, L.A. Clark, Q. Yang, M.A. Anderson, Environ. Sci. Technol. 30 (1996) 647.
[8] S. Yoshida, S. Takenaka, T. Tanaka, H. Hirano, H. Hayashi, Eleventh International Congress on Catalysis, Stud. Sur. Sci. Catal. 101 (1996) 871.
[9] S. Imamura, H. Tarumoto, S. Ishida, Ind. Eng. Chem. Res. 28 (1989) 1449.
[10] S. Imamura, T. Higashihara, H. Jindai, Chem. Lett. (1993) 1667.
[11] T. Liu, T. Cheng, Catal. Today 26 (1995) 71.
[12] Z. Liu, J. Tabora, R.J. Davis, J. Catal. 149 (1994) 117.
[13] J.B. Miller, S.T. Johnston, E.I. Ko, J. Catal. 150 (1994) 311.
[14] E.I. Ko, J.P. Chen, J.G. Weissman, J. Catal. 105 (1987) 511.
[15] M. Itoh, H. Hattori, K. Tanabe, J. Catal. 35 (1974) 225.
[16] H. Nakabayashi, Bull. Chem. Soc. Jpn. 65 (1992) 914.
[17] C. Contescu, V.T. Popa, J.B. Miller, E.I. Ko, J.A. Schwarz, Chem. Eng. J. 64 (1996) 265.
[18] A. Molnar, M. Bartok, M. Schneider, A. Baiker, Catal. Lett. 43 (1997) 123.
[19] P.K. Doolin, S. Alerasool, D.J. Zalewski, J.F. Hoffman, Catal. Lett. 25 (1994) 209.
[20] J.R. Sohn, J.H. Jang, J. Catal. 132 (1991) 563.
[21] W.F. Maier, J.A. Martens, S. Klein, J. Heilmann, R. Parton, K. Vercruysse, P.A. Jacobs, Angew. Chem. 108 (1996) 222.
[22] C.B. Khouw, C.B. Dartt, J.A. Labinger, M.E. Davis, J. Catal. 149 (1994) 195.
[23] A. Bendandi, G. Fornasari, M. Guidoreni, L. Kubelkova, M. Lucarini, F. Trifiro, Topic. Catal. 3 (1996) 337.
[24] R. Hutter, T. Mallat, A. Baiker, J. Catal. 153 (1995) 665.
[25] R. Hutter, T. Mallat, A. Baiker, J. Chem. Soc., Chem. Commun. (1995) 2487.
[26] Z. Liu, G.M. Crumbaugh, R.J. Davis, J. Catal. 159 (1996) 83.
[27] S. Imamura, T. Nakai, H. Kanai, T. Ito, Catal. Lett. 28 (1994) 277.
[28] S. Imamura, T. Nakai, H. Kanai, T. Ito, J. Chem. Soc., Faraday Trans. 91 (1995) 1261.
[29] S. Imamura, T. Nakai, H. Kanai, T. Shiono, K. Utani, Catal. Lett. 39 (1996) 79.
[30] S. Klein, S. Thorimbert, W.F. Maier, J. Catal. 163 (1996) 476.
[31] R. Hutter, T. Mallat, A. Baiker, J. Catal. 153 (1995) 177.
[32] R.A. Sheldon, J.A. Van Doorn, J. Catal. 31 (1973) 427.

[33] R.A. Sheldon, J. Mol. Catal. 7 (1980) 107.
[34] S. Klein, J.A. Martens, R. Parton, K. Vercruysse, P. Jacobs, W.F. Maier, Catal. Lett. 38 (1996) 209.
[35] A. Keshavaraja, V. Ramaswamy, H.S. Soni, A.V. Ramaswamy, P. Ratnasamy, J. Catal. 157 (1995) 501.
[36] S. Srinivasan, A.K. Datye, M. Hampden-Smith, I.E. Wachs, G. Deo, J.M. Jehng, A.M. Turek, C.H.F. Peden, J. Catal. 131 (1991) 260.
[37] S. Srinivasan, A.K. Datye, M.H. Smith, C.H.F. Peden, J. Catal. 145 (1994) 565.
[38] G. Deo, A.M. Turek, I.E. Wachs, D.R.C. Huybrechts, P.A. Jacobs, Zeolites 13 (1993) 365.
[39] M.A. Cauqui, J.J. Calvino, G. Cifredo, L. Esquivias, J.M. Rodriguez-Izquierdo, J. Noncryst. Solids 147 148 (1992) 758.
[40] M.P. McDaniel, M.B. Welsh, M.J. Dreiling, J. Catal. 82 (1983) 98.
[41] S.J. Conway, J.W. Falconer, C.H. Rochester, J. Chem. Soc., Faraday Trans. 1 85 (1989) 71.
[42] J.J. Calvino, M.A. Cauqui, G. Cifredo, L. Esquivias, J.A. Perez, J. Mater. Sci. 28 (1993) 2191.
[43] R. Mariscal, M. Galan-Fereres, J.A. Anderson, L.J. Alemany, J.M. Palacios, J.L.G. Fierro, in: G. Centi et al. (Eds.), Environmental Catalysis, SCI, Rome, 1995.
[44] B.E. Handy, A. Baiker, M. Schraml-Marth, A. Wokaun, J. Catal. 133 (1992) 1.
[45] B.M. Reddy, E.P. Reddy, B. Manohar, Appl. Catal. 96 (1993) L1.
[46] M. Galan-Fereres, R. Mariscal, L.J. Alemany, J.L.G. Fierro, J. Chem. Soc., Faraday Trans. 90 (1994) 3711.
[47] A.A. Elguezabal, V.C. Corberan, Catal. Today 32 (1996) 265.
[48] C.R. Dias, M.F. Portela, M. Galan-Fereres, M.A. Banares, M.L. Granados, M.A. Pena, J.L.G. Fierro, Catal. Lett. 43 (1997) 117.
[49] M. Atik, J. Zarzycki, J. Mater. Lett. 13 (1994) 1301.
[50] M. Atik, P.D.L. Neto, M.A. Aegerter, L.A. Avaca, J. Appl. Electrochem. 25 (1995) 142.
[51] K. Yu-Zhang, G. Boisjolly, J. Rivory, L. Kilian, C. Colliex, Thin Solid Films 253 (1994) 299.
[52] D. Zhu, T. Kosugi, J. Noncryst. Solids 202 (1996) 88.
[53] C.J. Brinker, G.W. Scherer, Sol–gel Science: The Physics and Chemistry of Sol–gel Processing, Academic Press, San Diego, CA, 1990.
[54] Z. Deng, E. Breval, C.G. Pantano, J. Noncryst. Solids 100 (1988) 364.
[55] E. Breval, Z. Deng, C.G. Pantano, J. Noncryst. Solids 125 (1990) 50.
[56] M. Aizawa, Y. Nosaka, N. Fujii, J. Noncryst. Solids 168 (1994) 49.
[57] T. Hayashi, T. Yamada, H. Saito, J. Mater. Sci. 18 (1983) 3137.
[58] S. Satoch, K. Susa, I. Matsuyama, J. Noncryst. Solids 146 (1992) 121.
[59] C. Contescu, V.T. Popa, J.B. Miller, E.I. Ko, J.A. Schwarz, J. Catal. 157 (1995) 244.
[60] D.T. On, L.L. Noe, L. Bonneviot, Chem. Commun. (1996) 299.
[61] P.J. Dirken, M.E. Smith, H.J. Whitfield, J. Phys. Chem. 99 (1995) 395.
[62] M. Schraml-Marth, K.L. Walther, A. Wokaun, B.E. Handy, A.J. Baiker, J. Noncryst. Solids 143 (1992) 93.
[63] K.L. Walther, A. Wokaun, B.E. Handy, A.J. Baiker, J. Noncryst. Solids. 134 (1992) 47.
[64] D.C.M. Dutoit, M. Schneider, A. Baiker, J. Catal. 153 (1995) 165.
[65] A.Y. Stakheev, E.S. Shpiro, J. Apijok, J. Phys. Chem. 97 (1993) 5668.
[66] C.H. Hung, J.L. Katz, J. Mater. Res. 7 (1992) 1861.
[67] S.M. Mukhopadhyay, S.H. Garofalini, J. Noncryst. Solids 126 (1990) 202.
[68] R.B. Greegor, F.W. Lytle, D.R. Sandstrom, J. Wong, P. Schultz, J. Noncryst. Solids 55 (1983) 27.
[69] A. Fernandez, A. Caballero, A.R. Gonzalez-Elipe, Surf. Interface Anal. 18 (1992) 392.
[70] A. Fernandez, A.R. Gonzalez-Elipe, C. Real, A. Caballero, G. Munuera, Langmuir 9 (1993) 121.
[71] A. Hanprasopwattana, T. Rieker, A.G. Sault, A.K. Datye, Catal. Lett. 45 (1997) 165.
[72] A. Hanprasopwattana, S. Srinivasan, A.G. Sault, A.K. Datye, Langmuir 12 (1996) 3173.
[73] M.G. Reichmann, A.T. Bell, Appl. Catal. 32 (1987) 315.
[74] A. Fernandez, J. Leyrer, A.R. Gonzalez-Elipe, G. Munuera, H. Knozinger, J. Catal. 112 (1988) 489.
[75] R. Castillo, B. Koch, P. Ruiz, B. Delmon, J. Catal. 161 (1996) 524.
[76] R. Mariscal, J.M. Palacios, M. Galan-Fereres, J.L.G. Fierro, Appl. Catal. A 116 (1994) 205.
[77] S. Haukka, E. Lakomaa, A. Root, J. Phys. Chem. 97 (1993) 5085.
[78] B.A. Morrow, A.J. Mcfarlan, J. Noncryst. Solids 120 (1990) 61.
[79] J. Klaas, G. Schulz-Ekloff, N.I. Jaeger, J. Phys. Chem. B 101 (1997) 1305.
[80] M. Galan-Fereres, L.J. Alemany, R. Mariscal, M.A. Banares, J.A. Anderson, J.L.G. Fierro, Chem. Mater. 7 (1995) 1342.
[81] Z. Liu, R.J. Davis, J. Phys. Chem. 98 (1994) 1253.
[82] M. Aizawa, Y. Nosaka, N. Fujii, J. Noncryst. Solids 128 (1991) 77.
[83] M. Toba, F. Mizukami, S. Niwa, T. Sano, K. Maeda, A. Annila, V. Komppa, J. Mol. Catal. 91 (1994) 227.
[84] M.F. Best, R.A. Condrate, J. Mater. Sci. Lett. 4 (1985) 994.
[85] S. Bordiga, S. Coluccia, C. Lamberti, L. Marchese, A. Zecchina, F. Boscherini, F. Buffa, F. Genoni, G. Leofanti, G. Petrini, G. Vlaic, J. Phys. Chem. 98 (1994) 4125.
[86] A. Chmel, G.M. Eranosyan, A.A. Kharshak, J. Noncryst. Solids 146 (1992) 213.
[87] I.M.M. Salvado, J.M.F. Navarro, J. Noncryst. Solids 147 148 (1992) 256.
[88] C.C. Perry, X. Li, D.N. Waters, Spectrochim. Acta 47A (1991) 1487.
[89] M.E. Smith, H.J. Whitfield, J. Chem. Soc., Chem. Commun. 6 (1994) 723.

[90] I. Grohmann, W. Pilz, G. Walther, H. Kosslick, V.A. Tuan, Surf. Interface Anal. 22 (1994) 403.
[91] J.K. Walters, J.S. Rigden, P.J. Dirken, M.E. Smith, W.S. Howells, R.J. Newport, Chem. Phys. Lett. 264 (1997) 539.
[92] J.S. Rigden, R.J. Newport, M.E. Smith, P.J. Dirken, G. Bushnell-Wye, J. Mater. Chem. 6 (1996) 337.
[93] S. Klein, B.M. Weckhuysen, J.A. Martens, W.F. Maier, P.A. Jacobs, J. Catal. 163 (1996) 489.
[94] L.L. Noc, D.T. On, S. Solomykina, B. Echchahed, F. Beland, C.C.D. Moulin, L. Bonneviot, Eleventh International Congress on Catalysis, Stud. Sur. Sci. Catal. 101 (1996) 611.
[95] D.R. Sandstrom, F.W. Lytle, P.S.P. Wei, R.B. Greegor, J. Wong, P. Schultz, J. Noncryst. Solids 41 (1980) 201.
[96] S. Pei, G.W. Zajac, J.A. Kaduk, J. Faber, B.I. Boyanov, D. Duck, D. Fazzini, T.I. Morrison, D.S. Yang, Catal. Lett. 21 (1993) 333.
[97] A.B. Rosenthal, S.H. Garofalini, J. Noncryst. Solids 107 (1988) 65.
[98] C. Kormann, D.W. Bahnemann, M.R. Hoffmann, J. Phys. Chem. 92 (1988) 5196.
[99] C.K. Jørgensen, Morden Aspects of Ligand Field Theory, North Holland, Amsterdam, 1971.
[100] M.R. Boccuti, K.M. Rao, A. Zecchina, G. Leofanti, G. Petrini, Stud. Surf. Sci. Catal. 48 (1989) 133.
[101] J.A. Duffy, Struct. Bonding (Berlin) 32 (1977) 147.
[102] X. Gao, I.E. Wachs, J. Phys. Chem. B 102 (1998) 5653.
[103] G. Lassaletta, A. Fernandez, J.P. Espinos, A.R. Gonzalez, J. Phys. Chem. 99 (1995) 1484.
[104] J.A. Mejias, V.M. Jimenez, G. Lassaletta, A. Fernandez, J.P. Espinos, A.R. Gonzalez, J. Phys. Chem. 100 (1996) 16255.
[105] T. Nakayama, J. Electrochem. Soc. 141 (1994) 237.
[106] N. Brun, C. Colliex, J. Rivory, K. Yu-Zhang, Microsc. Microanal. Microstruct. 7 (1996) 161.
[107] D. Scarano, A. Zecchina, S. Bordiga, F. Geobaldo, G. Spoto, G. Petrini, G. Leofanti, M. Padovan, G. Tozzola, J. Chem. Soc., Faraday Trans. 89 (1993) 4123.
[108] C. Cartier, C. Lortie, D. Trong On, H. Dexpert, L. Bonneviot, Physica B 208 209 (1995) 653.
[109] I.D. Brown, K.K. Wu, Acta Cryst. B 32 (1976) 1957.
[110] M.A. Roberts, G. Sankar, J.M. Thomas, R.H. Jones, H. Du, J. Chen, W. Pang, R. Xu, Nature 381 (1996) 401.
[111] F. Farges, G.E. Brown Jr., J.J. Rehr, Geochim. Cosmochim. Acta 60 (1996) 3023.
[112] F. Farges, G.E. Brown Jr., A. Navrotsky, H. Gan, J.J. Rehr, Geochim. Cosmochim. Acta 60 (1996) 3039.
[113] F. Farges, G.E. Brown Jr., J.J. Rehr, Phys. Rev. B 56 (1997) 1809.
[114] K.S. Kim, M.A. Barteau, W.E. Farneth, Langmuir 4 (1988) 533.
[115] T. Maschmeyer, F. Rey, G. Sanker, J.M. Thomas, Nature 378 (1995) 159.
[116] A.I. Biaglow, R.J. Gorte, S. Srinivasan, A.K. Datye, Catal. Lett. 13 (1992) 313.
[117] T. Nakayama, K. Onisawa, M. Fuyama, M. Hanazono, J. Electrochem. Soc. 139 (1992) 1204.
[118] H. Nakabayashi, N. Kakuta, A. Ueno, Bull. Chem. Soc. Jpn. 64 (1992) 2428.
[119] T. Kataoka, J.A. Dumesic, J. Catal. 112 (1988) 66.
[120] H. Nakabayashi, Bull. Chem. Soc. Jpn. 65 (1992) 914.
[121] K. Tanabe, T. Sumiyoshi, K. Shibata, T. Kiyoura, J. Kitagawa, Bull. Chem. Soc. Jpn. 47 (1974) 1064.
[122] B. Notari, Catal. Today 18 (1993) 163.
[123] R.A. Sheldon, J. Dakka, Catal. Today 19 (1994) 215.
[124] M.I. Zaki, H. Knozinger, Spectrochim. Acta A 43 (1987) 1455.
[125] S. Imamura, S. Ishida, H. Tarumoto, Y. Saito, T. Ito, J. Chem. Soc., Faraday Trans. 89 (1995) 757.
[126] D. Trong On, L. Bonneviot, A. Bittar, A. Sayari, S. Kaliaguine, J. Mol. Catal. 74 (1992) 233.